ACS APPLIED MATERIALS & INTERFACES

Research Article

www.acsami.org

# Solvent Control of Surface Plasmon-Mediated Chemical Deposition of Au Nanoparticles from Alkylgold Phosphine Complexes

Christopher L. Muhich,[†] Jingjing Qiu,[‡] Aaron M. Holder,[†,§,∥] Yung-Chien Wu,[‡] Alan W. Weimer,[†] Wei David Wei,[‡] Lisa McElwee-White,[‡] and Charles B. Musgrave*[,†,§]

[†]Department of Chemical and Biological Engineering, University of Colorado, 3415 Colorado Avenue, UCB 596, Boulder, Colorado 80309-0596, United States

[‡]Department of Chemistry and Center for Nanostructured Electronic Materials, University of Florida, 214 Leigh Hall, Gainesville, Florida 32611-7200, United States

[§]Department of Chemistry and Biochemistry, University of Colorado, UCB 215, Boulder, Colorado 80309-0215, United States

Supporting Information

**ABSTRACT:** Bottom-up approaches to nanofabrication are of great interest because they can enable structural control while minimizing material waste and fabrication time. One new bottom-up nanofabrication method involves excitation of the surface plasmon resonance (SPR) of a Ag surface to drive deposition of sub-15 nm Au nanoparticles from $MeAuPPh_3$. In this work we used density functional theory to investigate the role of the $PPh_3$ ligands of the Au precursor and the effect of adsorbed solvent on the deposition process, and to elucidate the mechanism of Au nanoparticle deposition. In the absence of solvent, the calculated barrier to $MeAuPPh_3$ dissociation on the bare surface is <20 kcal/mol, making it facile at room temperature. Once adsorbed on the surface, neighboring MeAu fragments undergo ethane elimination to produce Au adatoms that cluster into Au nanoparticles. However, if the sample is immersed in benzene, we predict that the monolayer of adsorbed solvent blocks the adsorption of $MeAuPPh_3$ onto the Ag surface because the $PPh_3$ ligand is large compared to the size of the exposed surface between adsorbed benzenes. Instead, the Au−P bond of $MeAuPPh_3$ dissociates in solution ($E_a$ = 38.5 kcal/mol) in the plasmon heated near-surface region followed by the adsorption of the MeAu fragment on Ag in the interstitial space of the benzene monolayer. The adsorbed benzene forces the Au precursor to react through the higher energy path of dissociation in solution rather than dissociatively adsorbing onto the bare surface. This requires a higher temperature if the reaction is to proceed at a reasonable rate and enables the control of deposition by the light induced SPR heating of the surface and nearby solution.

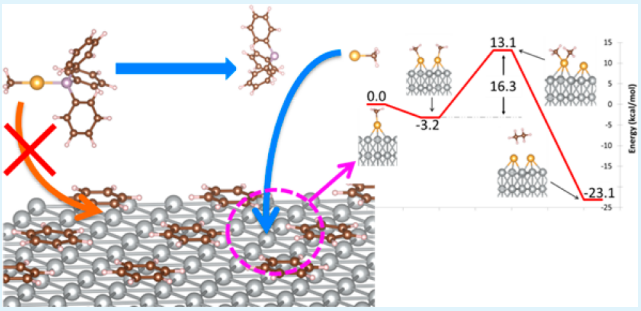


**KEYWORDS:** *bottom-up nanofabrication, preferential molecular adsorption, thermal decomposition, organometallic chemistry, organogold chemistry, density functional theory*

## 1. INTRODUCTION

Nanomaterials with controlled size and shape, especially in the sub-15 nm regime, find applications in a variety of areas, including catalysis and sensing.[1−4] Among them, noble metal nanoparticles (NPs), such as Au and Ag, are attracting increasing attention due to their dual roles as catalysts and light concentrators.[5−7] For instance, catalytically active Au NPs can be loaded on substrates for *in situ* photochemical reaction and detection.[8,9] To achieve such composite structures, seed-mediated wet chemical methods are often used.[9] However, it is difficult to obtain surfactant-free NPs with controlled size using such methods. Wei and McElwee-White have recently reported a surface plasmon-mediated chemical solution deposition (SPMCSD) method to grow sub-15 nm Au NPs on a nanostructured Ag surface.[10] In a typical SPMCSD experiment, a Ag film on a nanosphere substrate (AgFON) is submerged into a benzene solution containing methyl(triphenylphosphine) gold ($MeAuPPh_3$). Upon illumination with broadband visible light, the excitation of the surface plasmon resonance (SPR) of the AgFON substrate raises the surface temperature to over 230 °C, while the mean temperature of the solution remains under 40 °C during the reaction.[10,11] The rise in surface temperature leads to $MeAuPPh_3$ decomposition, producing Au nanoparticles on the AgFON substrate with concomitant generation of ethane and loss of phosphine.[10,11]

To enable mechanism-based precursor design[12,13] for SPMCSD, it is necessary to determine the fundamental mechanism of the deposition process. First-principles quantum

Received: March 3, 2015
Accepted: June 3, 2015
Published: June 3, 2015





DOI: 10.1021/acsami.5b01918
ACS Appl. Mater. Interfaces 2015, 7, 13384−13394

chemical modeling can provide detailed descriptions of the possible reaction mechanisms, including information not readily available from experiment such as the nature of transition states and intermediates. For instance, the energies and atomic and electronic structures of transition states and intermediates along various possible reaction pathways provide insight into the mechanism of SPMCSD and how precursors and conditions might be designed for SPMCSD processes. Decomposition of the Au precursor and nanoparticle deposition could proceed through routes where the SPR provides thermal energy for the decomposition of precursor molecules on the Ag surface or in nearby solution, or alternatively, where $MeAuPPh_3$ dissociation is activated by SPR modification of the electronic structure of the precursor or the substrate. This contribution reports density functional theory (DFT) calculated reaction energies and activation barriers of the thermally activated pathways, both in solution and on the Ag surface, in order to investigate whether the thermally activated decomposition of $MeAuPPh_3$ is a viable mechanism for SPMCSD if the SPR acts solely as a heating mechanism.

Furthermore, we investigated the role that the solvent plays in the SPMCSD of Au NP deposition. It has been previously shown that solvents can affect the reaction rates and selectivity of surface reactions occurring at liquid−solid interfaces, for example, in heterogeneous catalysis.[14] Therefore, it is important to consider the roles of solvent in the mechanism of SPMCSD. At the liquid−solid interface solvent molecules can directly adsorb to and/or form structured multilayers on the catalyst. These interfacial structures can act as solvent diffusion barriers that limit the transport of reactants to or across the catalyst surface;[15−17] alter the preferential adsorption geometry of the reactant(s);[18] affect the relative stabilities of reactants, intermediates, transition states, and products;[18] and thus significantly influence the thermodynamics and kinetics of catalytic processes. Most relevant to this study, competitive adsorption of solvent molecules or dissociation fragments may block reactive sites and thus alter reaction rates and selectivity.[19−22]

In this work, we show that adsorbed benzene solvent molecules block the $MeAuPPh_3$ precursor from adsorbing to the Ag surface during the SPMCSD process. Consequently, the rate-limiting step of Au deposition from $MeAuPPh_3$ by SPMCSD in benzene is the decomposition of the precursor in solution. This enables the control of the organometallic precursor decomposition and Au nanoparticle formation by localized heating via SPR excitation and, potentially, altering the decomposition energetics of the precursor through electronic excitation of solution-phase $MeAuPPh_3$. In contrast, SPMCSD by SPR-mediated localized heating is not expected to enable control of nanoparticle deposition for cases where precursor adsorption outcompetes solvent adsorption.

## 2. METHODS

Both discrete molecular and extended periodic boundary condition quantum chemical calculations were performed on model systems for the SPMCSD of Au nanoparticles. The GAMESS molecular quantum chemistry suite was used to conduct solution-phase calculations.[23] Calculations were performed with the M06 meta-hybrid DFT functional[24] and SBKJC[25,26] effective core pseudopotential and 6-31G** basis set. The M06 density functional was chosen because it has been shown to accurately predict Au cluster structures and energies.[27] The SBKJC pseudopotential was employed to reduce the number of Au electrons in the system and make the computations more tractable. A polarizable continuum model (PCM)[28] parametrized for benzene was used to model the solvent.

Periodic boundary condition (PBC) DFT calculations were executed using the Vienna *Ab Initio* Simulation Package (VASP)[29,30] and employed projector augmented wave (PAW) pseudopotentials.[31,32] PAWs treated H 1s, C 2s and 2p, P 3s and 3p, Ag 5s and 4d, and Au 6s and 5d electrons explicitly with a plane wave expansion. PBC DFT computations were performed using the optB88-vdW density functional (vdW-DF) which nonempirically and self-consistently accounts for the nonlocal van der Waals (vdW) interactions in the energy functional; optB88-vdW is based on the method of Dion et al.[33] as implemented in VASP. This functional was selected not only because it self-consistently evaluates the van der Waals energy, but because it also generally produces low mean absolute errors and resulted in a mean absolute error of 0.23 kcal/mol as compared to highly accurate CCSD(T) calculations of the S22 data set.[34] We found that optB88-vdW predicts the mean energy for $MeAuPPh_3$ on Ag of the predicted adsorption energies calculated using other Dion-based functionals (optPBE and optB86b), as shown in Supporting Information Table S1.

A convergence test of the effect of cutoff energies found only a 0.05 kcal/mol difference in the $MeAuPMe_3$ (a model gold phosphine complex) adsorption energy to the bare (111) silver surface for plane wave expansions with 400 and 500 eV cutoff energies; therefore, we utilized the less computationally expensive 400 eV cutoff energy. Two different supercells were used to model the silver surface, a smaller 4 × 4 supercell and a larger 6 × 6 supercell. We modeled the Ag surface as an FCC Ag(111) surface because this is the most stable Ag surface. An oxidized (AgO) surface was not considered because the experimental Ag surfaces did not show significant oxidation.[10] Additionally, the surface plasmons may reduce any AgO present on the surface, similar to the reduction of $Cu_2O$ upon SPR excitation.[35] Both cells were four atomic layers thick where the bottom two layers of the slab were frozen to represent the bulk, while the top two layers were allowed to completely relax. At least 15 Å of vacuum space between the top of the slab and the frozen backside was used in slab-based calculations. Calculations were carried out with a 4 × 4 × 1 Γ-point centered Monkhorst−Pack-based k-point mesh for the small slab while Γ-point calculations were performed for the larger slab due to the increased computational cost of DFT-vdW methods. Furthermore, extensive Brillouin zone folding in the case of large supercells effectively reduces the need for explicit k-point sampling. The smaller 4 × 4 × 1 slab was used for calculations of surface reactions involving ethane elimination, and adsorption of a single benzene or MeAu, while the larger 6 × 6 × 1 cell was used to model adsorption of the $MeAuPPh_3$ precursor, its dissociation on the surface, and the benzene monolayer. Geometry optimizations were performed using the quasi-Newton−Raphson method. The NEB method[36] was utilized to locate transition states and calculate their associated barriers for surface reactions modeled using periodic slabs.

Molecular adsorption energies were calculated using the expression

$$E_{ads} = E_{system} - (E_{surf} - E_{mol})$$

where $E_{ads}$ is the adsorption energy of the molecule, $E_{system}$ is the total energy of the molecule adsorbed on the silver surface, and $E_{surf}$ and $E_{mol}$ are the energies of the bare surface and of the organic molecule, respectively. Note that a negative energy indicates that adsorption is exothermic. Energies are reported as enthalpies at 0 K in kcal/mol for all reactions and activation barriers unless otherwise noted.

## 3. RESULTS

In order for the deposition of Au nanoparticles on the Ag surface to occur, both the methyl and the phosphine ligands must dissociate from the Au atom of the $MeAuPPh_3$ precursor, and Au atoms must bond to the Ag surface. Various routes could result in Au adatoms on the Ag surface including the following: (1) dissociation of one ligand from the solvated precursor followed by adsorption of the Au containing


DOI: 10.1021/acsami.5b01918
ACS Appl. Mater. Interfaces 2015, 7, 13384−13394

fragment, (2) molecular adsorption and subsequent dissociation of the precursor, or (3) dissociative adsorption of the precursor. Deposition of organogold fragments onto the surface by any of these three basic mechanisms requires additional surface reactions to eliminate the remaining organic moieties and form free Au adatoms. After Au adatoms are produced, they are able to migrate across the Ag surface and cluster to form nanoparticles. All three basic deposition mechanisms require adsorption, either of the intact precursor, or of its dissociation fragments. For the cases of molecular adsorption of the precursor followed by dissociation on the surface and dissociative adsorption, adsorption requires several adjacent bare surface sites given the large size of $MeAuPPh_3$. Consequently, we studied the desorption of adsorbed benzene solvent molecules because this may be a critical step in the SPMCSD process that affects the energetics of the various mechanisms depending on the number of bare Ag surface sites required for adsorption. We did not examine the formation of Au nanoparticles from Au atoms on the surface because this process is exothermic,[37] and the diffusion of Au on Au, which is likely similar to the diffusion of Au on Ag due to analogous migration mechanisms and lattice spacing, is relatively facile even at room temperature.[38,39] Therefore, Au cluster formation from individual Au atoms is unlikely to be the rate-determining step in SPMCSD. We report the results of our investigation of the mechanism of SPMCSD of Au NPs on Ag by first describing benzene desorption in relation to $MeAuPPh_3$ adsorption.

**3.1. Effects of Adsorbed Solvent on Precursor Decomposition on the Ag Surface.** In SPMCSD of Au NPs on Ag, the Ag surface is submerged in a benzene solution containing solvated $MeAuPPh_3$ molecules. Therefore, we investigated the interaction of benzene with the Ag surface as benzene and other aromatics are known to adsorb on metal surfaces.[40−43] We considered a low surface area coverage of benzene on the Ag(111) surface where benzene adsorbs flat on the surface, as shown in Figure 1a. This represents a more favorable configuration for precursor adsorption because at higher surface coverages benzene adsorbs end-on in a tilted geometry and more benzene molecules must be displaced to provide sufficient bare surface to enable precursor adsorption; the implications of higher coverages are discussed below. Benzene molecules interact favorably with the Ag surface through van der Waals interactions, and we calculate an adsorption energy of 14.3 kcal/mol with each benzene lying flat on the surface covering an area of approximately 16 $Å^2$. Our predicted adsorption energy is similar to the experimentally determined adsorption energy of benzene on Ag(111) of 12−13 kcal/mol,[44] suggesting that benzene forms an adsorbed monolayer on the Ag surface that exchanges slowly with benzene molecules in solution. A uniform benzene monolayer covers the majority of the top and bridging sites[44] as shown in Figure 1 and leaves mostly 3-fold hollow sites exposed within the interstitial space between adsorbed benzene molecules available for adsorption unless benzene molecules desorb or rotate from their planar adsorption geometry on the Ag(111) surface.

The adsorbed $MeAuPPh_3$ covers a relatively large area (~45 $Å^2$) on the Ag(111) surface (see Figure 1b); when adsorbed in the flat configuration at least three contiguous benzene molecules must desorb to allow for the adsorption of $MeAuPPh_3$, which is unlikely. Although the surface temperature generated by SPR-mediated photothermal heating (~230 °C)

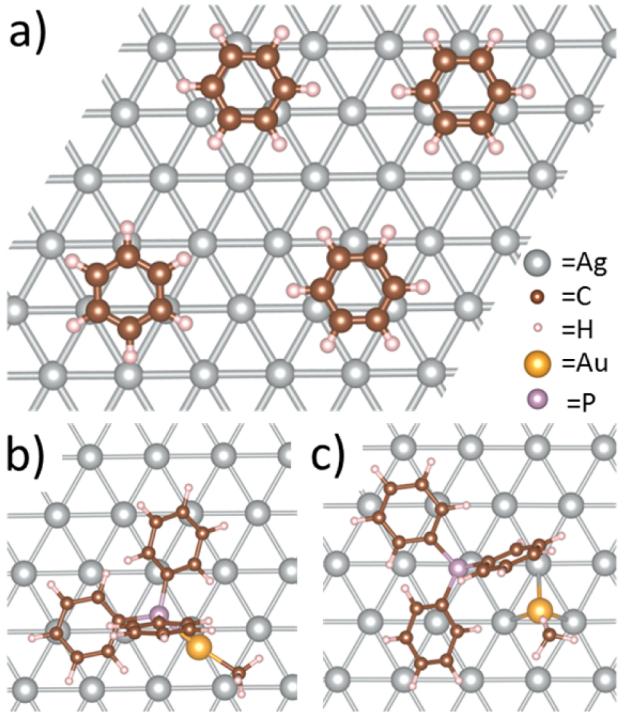


**Figure 1.** Structures of adsorbed species on the Ag(111) surface: (a) adsorbed benzene monolayer, (b) the molecularly adsorbed $MeAuPPh_3$ precursor, and (c) the adsorbed MeAu and $PPh_3$ fragments of the disociated $MeAuPPh_3$ precursor. The small white, medium brown, medium purple, large silver, and large yellow spheres represent H, C, P, Ag, and Au atoms, respectively.

is high enough to activate benzene desorption (roughly one out of every $2.4 \times 10^6$ benzene adsorption sites will be vacant), it is unlikely that three neighboring benzene adsorption sites would be vacant simultaneously due to the high entropic and enthalpic costs of this configuration. At the benzene vacancy density at 230 °C, we calculate a configurational entropy penalty to arrange three vacancies next to one another of roughly 63 cal/mol K, which corresponds to a ~ 32 kcal/mol entropic penalty to the free energy. For a description of how the configurational entropy loss was estimated, see the Supporting Information. This indicates that finding three adjacent vacancies is extremely unlikely, and thus that a near-surface $MeAuPPh_3$ would rarely encounter a sufficiently large area of bare Ag(111) surface to adsorb. From an enthalpic perspective, $MeAuPPh_3$ adsorbs on Ag(111) with an adsorption energy of only −38.5 kcal/mol, as shown in Figure 1b, while the adsorption energy of each benzene molecule is −14.3 kcal/mol. Thus, the displacement of three benzene molecules by a precursor molecule is endothermic by 4.4 kcal/mol. Therefore, the overall free energy of $MeAuPPh_3$ molecular adsorption is 35.9 kcal/mol at 230 °C with a free energy activation barrier of 74.6 kcal/mol. The activation barrier is considered to be the free energy of desorption of three neighboring benzene molecules. The dissociation of the Au−P bond of an adsorbed $MeAuPPh_3$ would require additional bare surface sites and thus desorption of additional benzene molecules, making this process unlikely. For experimental benzene surface coverages higher than the low surface density considered here, the free energies are lower than the low density configuration. Therefore, the free energy penalty for displacement of adsorbed benzene molecules by a precursor molecule is more prohibitive at higher benzene


DOI: 10.1021/acsami.5b01918
ACS Appl. Mater. Interfaces 2015, 7, 13384−13394

coverages, which is already exergonically unfavorable by $\Delta G$ = 35.9 kcal/mol. These factors make pathways that involve $MeAuPPh_3$ adsorption rare, and therefore, the majority of $MeAuPPh_3$ decomposition must occur in solution; these predictions agree with the experimental observation that no phosphine groups are adsorbed to the surface after SPMCSD.[10]

**3.2. Solution-Phase Precursor Decomposition.** We investigated several possible solution-phase $MeAuPPh_3$ decomposition reactions which produce fragments that might adsorb to the Ag surface. These include phosphine and methyl group dissociation from the $MeAuPPh_3$ precursor as well as removal of the methyl groups of two $MeAuPPh_3$ molecules by binuclear reductive elimination. Kochi et al. experimentally investigated the solution-phase decomposition of $MeAuPPh_3$ and determined that the observed kinetics are consistent with phosphine loss as the rate-determining step.[45]

We investigated the reaction pathway for Au−P dissociation, and ethane reductive elimination between two precursors, as shown in Figure 2. The calculated Au−P dissociation barrier

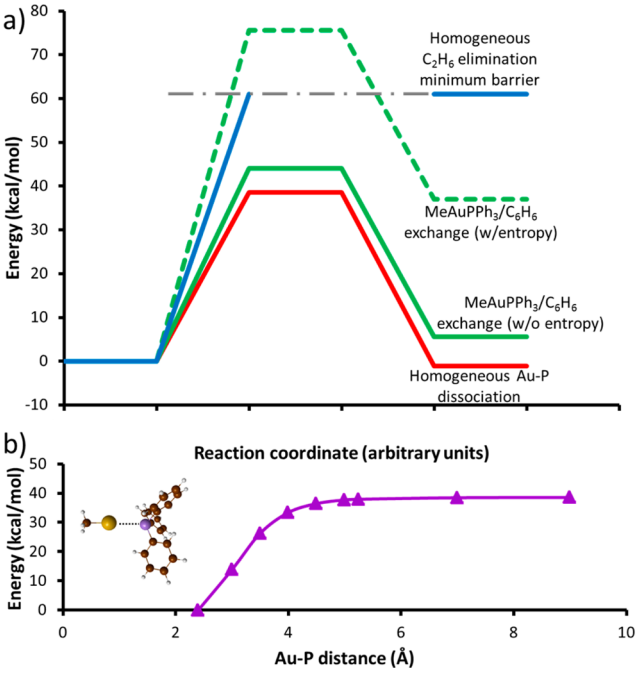


**Figure 2.** (a) Relative energies along the reaction paths for solution-phase $MeAuPPh_3$ dissociation and adsorption. The plotted dissociation pathways are solution-phase ethane elimination (blue), the exchange of a solution-phase $MeAuPPh_3$ molecule for three neighboring benzene molecules adsorbed on the Ag(111) surface excluding (green) and inluding (dashed green) configurational entropic effects, and solution-phase Au−P dissociation and subsequent MeAu adsorption (red). (b) The relative energy of $MeAuPPh_3$ as the Au−P bond dissociates. Because Au−P dissociation involved no transition state, the activation and reaction energies are identical for Au−P bond cleavage. The small white, medium brown, medium purple, and large yellow spheres represent H, C, P, and Au atoms, respectively.

and reaction energy is 38.5 kcal/mol while we obtain reaction energies of 61.0 and 76.7 kcal/mol for reductive elimination of ethane and Au−$CH_3$ dissociation, respectively. The high reaction energies of solution-phase ethane elimination and Me−Au bond scission suggest that Au−P bond scission is the preferred solution-phase reaction, and consequently, we chose to not search for possible higher lying solution-phase ethane elimination or Au−Me dissociation transition states. Thus, our results suggest that at the reaction temperature solution-phase Au−P dissociation is operative, while reductive elimination and Au−C dissociation are not competitive. These results are consistent with previous experimental observations that determined that Au−P dissociation is the rate-limiting step in solution-phase decomposition.[45]

SPR can drive chemical processes by transferring electrons to/from or exciting adsorbed and near-surface reactants in addition to providing thermal energy.[6,46] SPR excites surface electrons to produce nonthermal distributions with larger electron densities at higher energies than those described by a Fermi−Dirac distribution. This increases the electronic populations of surface states at energies at which electrons have sufficient energy to transfer to near-surface precursor molecules. Because the LUMO of $MeAuPPh_3$ is only roughly 2 eV above the 0 K ground state Fermi energy, SPR excited electrons likely transfer to near-surface solution-phase $MeAuPPh_3$ molecules in regions with significant electric field enhancements. The Au−P dissociation reaction energy of one-electron-reduced $MeAuPPh_3$ is lowered to 27.2 kcal/mol. The lowering of the Au−P dissociation energy upon reduction is consistent with experimental observations of the electrochemistry of gold complexes.[47] Accordingly, in the cyclic voltammogram of $MeAuPPh_3$ (Supporting Information Figure SI1), the first reduction wave is irreversible, as expected for facile phosphine dissociation. This suggests that SPR plays a dual role in enabling SPMCSD: (1) elevating the near-surface solution temperature which provides the energy necessary for Au−P bond scission and (2) accelerating this reaction in regions with high populations of SPR excited electrons by reducing the precursor and facilitating reaction through the lower barrier pathway (relative to the nonreduced precursor). Because neutral precursor dissociation is likely active at the near-surface temperatures of SPR and is a worst case scenario for the Au−P dissociation path, we will continue our discussion on the basis of the 38.5 kcal/mol barrier for neutral $MeAuPPh_3$ dissociation; however, we note that, as we have just demonstrated, the reaction barriers could be lower, particularly in regions with significant field enhancement.

The lower barrier for Au−P dissociation relative to Au−C dissociation arises because the Au−P bond (38.5 kcal/mol) is weaker than the Au−C bond (76.7 kcal/mol). In fact, the phosphine ligand strengthens the Au−C bond, as demonstrated by the fact that the Au−C dissociation energy is only 61.2 kcal/mol in the absence of the phosphine ligand, 15.4 kcal/mol weaker than when the phosphine ligand is bound. The larger bond strength comes from the donation of electron density from phosphine to the Au atom, which in turn donates electron density to the attached methyl C atom, leaving the Au and C atoms with atomic charges of −0.12 and −0.32 $e^-$ as determined by a population analysis using the CHELPG algorithm.

Unlike the $MeAuPPh_3$ precursor, the dissociated MeAu species is small enough to adsorb at exposed 3-fold hollow sites in the interstitial space between adsorbed benzene molecules of the uniform benzene monolayer on the Ag(111) surface, as shown in Figure 3a. Therefore, MeAu adsorbs onto the Ag surface without desorption of benzene molecules. The Au atom of adsorbed MeAu bonds to the Ag atoms of a Ag(111) hollow site resulting in adsorption energies of 44.0 and 39.6 kcal/mol with and without coadsorbed benzene molecules, respectively,


DOI: 10.1021/acsami.5b01918
ACS Appl. Mater. Interfaces 2015, 7, 13384−13394

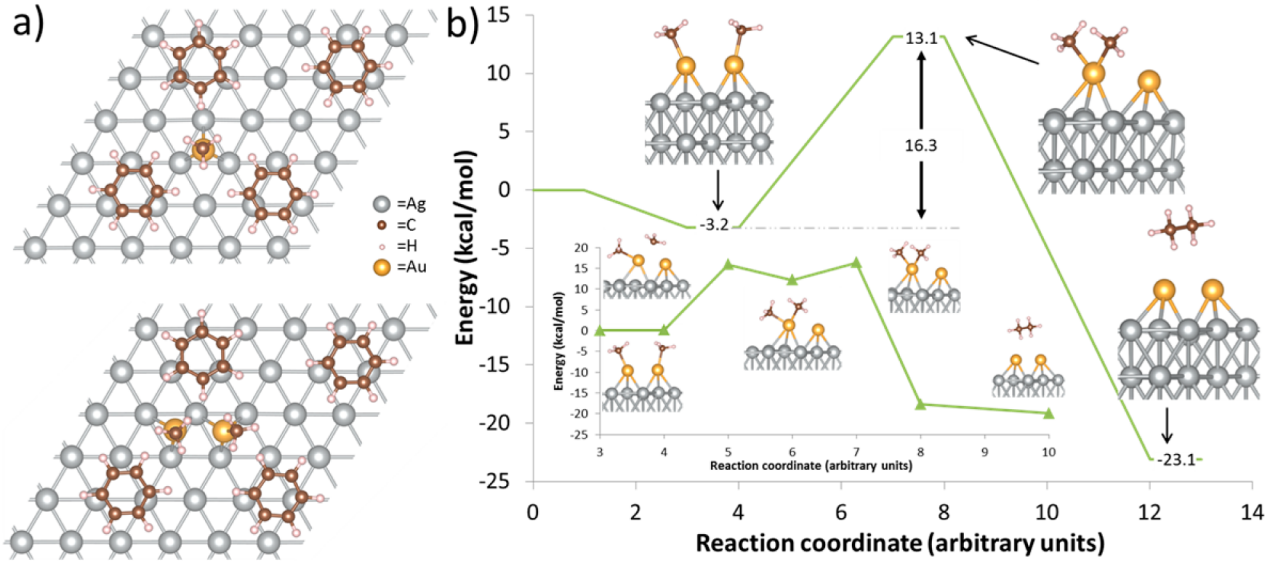


**Figure 3.** (a) Structures of adsorbed MeAu species on the Ag(111) surface between the molecules of a benzene monolayer. The figures show a single adsorbed MeAu (top) and a pair of adsorbed MeAu (bottom) molecules. (b) A schematic of the minimum energy path for surface ethane formation from neighboring adsorbed MeAu moieties. The inset shows the nudged elastic band pathway and the associated geometries for the ethane formation reaction. The small white, medium brown, large silver, and large yellow spheres represent H, C, Ag, and Au atoms, respectively.

where vdW interactions were described using the optB88-vdW method. The relatively small difference (4.4 kcal/mol) in the MeAu adsorption energies on the bare and benzene covered Ag surfaces compared to the adsorption energy of 44.0 kcal/mol indicates that the combined effects of vdW and steric interactions between the coadsorbed benzene and MeAu are minor compared to the electronic interactions between MeAu and the Ag surface. Consequently, for cases where the interstitial space between adsorbed benzenes is sufficiently large to allow for a species to adsorb, the bare Ag surface serves as a good model of the benzene coated Ag surface. Therefore, MeAu species produced near the surface from homogeneous phase Au−P dissociation readily adsorb to the Ag surface when they approach exposed sites. The 38.5 kcal/mol activation barrier for Au−P dissociation in solution and subsequent adsorption of the MeAu fragment indicate that this is a viable pathway at 230 °C, the minimum Ag surface temperature measured in the Au SPMCSD experiment.[10] It is worth noting that the temperature profile away from the Ag surface drops off precipitously and therefore limits decomposition of the precursor to the region near the Ag surface.

**3.3. Surface Au−Me Bond Scission and Ethane Formation.** Once MeAu dissociates from the $PPh_3$ ligand and adsorbs onto the surface, it must still undergo an additional Au−C bond scission to form Au adatoms. The methyl group of a MeAu species either reacts with a second, neighboring MeAu to form ethane directly, or the methyl group can dissociate from the Au atom onto the Ag surface leaving a Au surface atom. If methyl groups from MeAu transfer onto the Ag surface, they must react and desorb from the surface in order to prevent them from passivating the substrate by blocking Au atom diffusion and MeAu adsorption, or blocking Au nanoparticle surface migration. This could occur by C−C coupling reactions, or an overall galvanic displacement reaction,[48,49] as discussed below. Furthermore, on the Ag(111) surface covered by a complete benzene monolayer, neighboring hollow sites, top sites, and neighboring top and hollow sites are exposed in the interstitial space between adsorbed benzene molecules (Figure 1a). Therefore, ethane formation reactions to eliminate methyl groups may occur at these locations and at Au adatom sites on the benzene coated Ag surface.

*3.3.1. Surface MeAu−MeAu Ethane Elimination.* Bringing two adsorbed MeAu species together to occupy neighboring hollow sites on Ag(111) is nearly thermoneutral releasing only 3.2 kcal/mol on the bare surface and requiring 5.5 kcal/mol on the benzene covered surface (see Figure 3b). As noted above, the relatively small difference between these adsorption energies indicates that adsorbed benzenes do not significantly alter the behavior of two neighboring MeAu groups adsorbed in the interstitial space of the benzene coated Ag surface. In addition to the open reaction sites between adsorbed benzene molecules, the 14.3 kcal/mol desorption energy for a single benzene molecule and the relatively high reaction temperature suggest that benzene desorption makes additional surface sites available for reductive elimination of ethane from neighboring MeAu groups. Furthermore, open reaction sites created by benzene desorption enable MeAu to adsorb and react while only weakly interacting with neighboring adsorbed benzene molecules. Therefore, we only calculated ethane elimination on the uncoated Ag surface in the interest of computational efficiency. From two neighboring MeAu adsorbates two methyl groups can undergo a C−C coupling reaction to form ethane, which is exothermic by 23.1 kcal/mol and passes through a transition state with a 13.1 kcal/mol activation barrier referenced to the separated adsorbed MeAu species (Figure 3). This reaction proceeds through two steps: (1) transfer of one of the methyl groups from adsorbed MeAu to the Au atom of the neighboring MeAu to form $Me_2Au$ followed by (2) reductive elimination from $Me_2Au$ to form ethane. We find that the second step involves a larger activation energy, as shown in Figure 3b. A charge population analysis indicates that the methyl remains neutral as it transfers between Au atoms and that the Au atoms remain essentially neutral even in the metastable configuration in which both Me groups are bound to one of the Au atoms. The calculated structure of the $Me_2Au$


DOI: 10.1021/acsami.5b01918
ACS Appl. Mater. Interfaces 2015, 7, 13384−13394

species has an 86.0° C−Au−C bond angle, and a 2.15 Å C−Au bond length, which is elongated by 0.06 Å from the 2.09 Å C−Au bond length of adsorbed MeAu. The two methyl groups of the calculated structure are positioned so that the line through the two C atoms lies orthogonal to the line between the two Au atoms. The two methyl groups can bond to a single Au atom concurrently because the Au adatom sits above the plane of the Ag(111) surface, thus allowing the methyl groups to bend away from each other and toward the Ag surface plane without incurring significant steric hindrance with the surface; however, the remaining steric hindrance and slightly elongated C−Au bond result in $Me_2Au$ formation from two MeAu species being endothermic by 12.2 kcal/mol. As $Me_2Au$ forms, the methyl groups rotate such that the line between the two C atoms of $Me_2Au$ lies perpendicular to the line between the two Au atoms (Figure 3), whereas these two lines are nearly parallel to each other for two neighboring adsorbed MeAu species on Ag(111). Once the methyl groups dissociate from the Au atoms, the resulting Au dimer can either bind to free Au adatoms and grow into a Au nanoparticle or dissociate. Au dimer dissociation is endothermic by 4.1 kcal/mol, and produces individual Au adatoms that are free to diffuse across the surface and bind to other Au adatoms or clusters. The low barrier to ethane formation of only 13.1 kcal/mol relative to two adsorbed MeAu species (11.7 kcal/mol when referenced to two solution-phase $MeAuPPh_3$ precursor molecules) suggests that at the high temperatures present in SPMCSD this step is fast and that SPMCSD temperatures are not required for ethane elimination. This is also true for ethane formation on the bare surface within a benzene vacancy, which involves a barrier of 26.0 kcal/mol referenced to two solution-phase $MeAuPPh_3$ molecules and a benzene monolayer, although this reaction is expected to be sluggish at room temperature.

*3.3.2. Me Removal from Ag(111).* Ethane elimination reactions between two neighboring adsorbed MeAu species are not the only possible pathways to dissociate the C−Au bond; the Me group could transfer to the surface and form higher order alkane species via ethane elimination or a Fischer−Tropsch-like reaction, or the Me group could abstract surface Ag atoms in an overall Au/Ag galvanic displacement reaction. Our calculations predict a 22.7 kcal/mol activation barrier for methyl group transfer from the adsorbed MeAu species to the Ag(111) surface and that this step is endothermic by 12.9 kcal/mol. Similar to transfer of the methyl group between the Au atoms of neighboring MeAu species, the methyl migrates to the surface as a neutral species. The endothermicity for the transfer of the methyl group from MeAu to a Ag surface atom indicates that the C−Au bond is stronger than the C−Ag bond as indicated by the longer C−Ag bond ($d_{C-Ag}$ = 2.20 Å) compared to the C−Au bond ($d_{C-Au}$ = 2.09 Å). The stronger C−Au bond results from better orbital matching between the C $sp^3$ orbital and the contracted d-orbitals of Au relative to Ag which is caused by the lanthanide contraction between the second and third rows of the transition metals. Once the methyl group transfers from MeAu to the Ag surface, the Au adatom is free to migrate on the Ag surface to form Au nanoparticles. Consequently, this pathway serves as a second low energy path for Au nanoparticle formation that does not require neighboring adsorbed MeAu species.

Direct methyl reductive elimination to form ethane on the bare Ag(111) surface is exothermic by −44.8 kcal/mol and involves an activation barrier of 25.6 kcal/mol relative to two neighboring methyl groups on the Ag surface. Due to the cost of transferring a methyl group from MeAu to the Ag surface, these energies become $E_{rxn}$ = −19.0 and $E_a$ = 51.4 kcal/mol relative to two separated adsorbed MeAu species, as shown in Figure 4. On the Ag surface, ethane formation between two

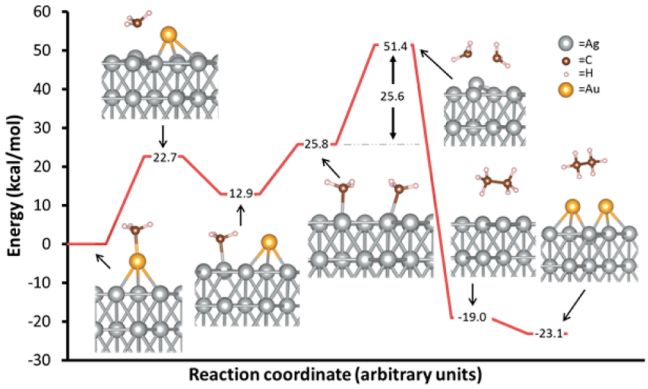


**Figure 4.** Schematic reaction path for the formation of ethane on the Ag surface referenced to two separated MeAu molecules on the Ag(111) surface. The small white, medium brown, large silver, and large yellow spheres represent H, C, Ag, and Au atoms, respectively.

neighboring adsorbed methyl groups does not involve the transfer of one methyl to the Ag atom of the neighboring MeAg site to form $Me_2Ag$ because this involves significant steric hindrance between the two methyl groups and between the methyl groups and the Ag surface as well as the oxidation of a Ag surface atom to the $Ag^{2+}$ state. Although two methyls are not able to form $Me_2Ag$, they do pull a Ag surface atom partially out of the surface plane as they rise off the surface and approach each other to form ethane. This enables the second methyl group to weakly bond to this Ag atom while dissociating from the Ag atom it was originally bound to (see the transition state shown in Figure 4). This allows the Me groups to rotate toward one another so that they are oriented in a direction that enables the formation of the C−C bond. Although the displacement of the Ag atom out of the surface plane strains its bonds to other Ag atoms, it increases the partial bonding between the methyls and the Ag atom and lowers steric repulsion between the methyls and Ag surface which lowers the barrier relative to the energetic cost of ethane formation by complete Me−Ag bond cleavage. At the transition state, the C−Ag bond lengths are 2.44 and 2.34 Å, the C−C bond length is 2.16 Å, and the C−Ag−C bond angle is 53.9°. The larger exothermicity of the ethane elimination reaction on Ag(111) relative to ethane elimination from neighboring MeAu species with respect to two neighboring methyl groups on Ag or Au, respectively, arises from the weaker Me−Ag bond, and consequently the higher initial state energy. Ethane elimination from adsorbed methyls on Ag(111) produced by dissociation of separated adsorbed MeAu species is 4.1 kcal/mol higher in energy than ethane elimination from neighboring adsorbed MeAu species (shown in Figure 4) that directly produces a Au dimer because Au dimer formation from Au adatoms on Ag(111) is exothermic by 4.1 kcal/mol. However, the free Au atoms produced by the Ag-based pathway eventually add to other Au clusters, eliminating this energy difference. The 51.4 kcal/mol activation barrier suggests that ethane formation on Ag is likely not competitive with Au-based ethane elimination even at the relatively high temperatures obtained in SPMCSD.


DOI: 10.1021/acsami.5b01918
ACS Appl. Mater. Interfaces 2015, 7, 13384−13394

Another possible mechanism for removing methyls from the Ag surface is analogous to Fischer–Tropsch catalysis[50−52] where the adsorbed methyls dissociate into fragments that subsequently undergo C–C bond formation to form $C_2$ and higher hydrocarbons. The first step of methyl decomposition is the dissociation of a single H from a methyl to form a surface H and a methylene ($CH_2$) group. We find that not only does this reaction involve a high activation energy of 45.3 kcal/mol (58.2 kcal/mol), but also it is endothermic by 25.0 kcal/mol (38.0 kcal/mol) with respect to a Me group (or an adsorbed MeAu species) on the Ag(111) surface, as shown in Figure 5. Even at

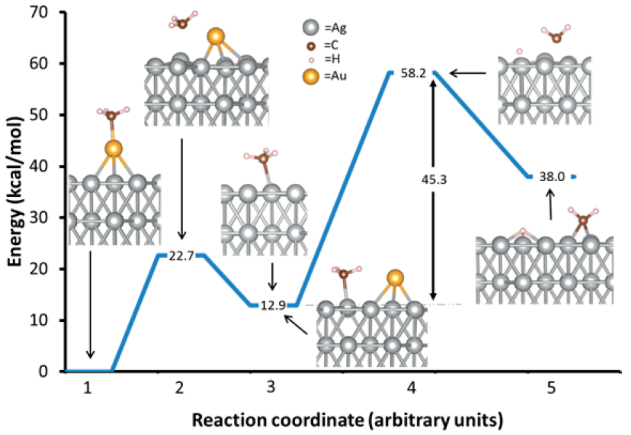


**Figure 5.** Schematic reaction path for the decomposition of MeAu on the Ag(111) surface. The structures shown at reaction coordinate 3 illustrate the final geometry of MeAu dissociation (bottom) and initial geometry of Me dissociation (top). The small white, medium brown, large silver, and large yellow spheres represent H, C, Ag, and Au atoms, respectively.

230 °C this means that only $1.3 \times 10^{-9}$ % of surface Me groups are decomposed at equilibrium. Additionally, the overall activation barrier for the first step of the methyl decomposition pathway is higher by 6.8 and 45.1 kcal/mol relative to the ethane elimination reactions on Ag and Au, respectively; therefore, we did not further investigate methyl decomposition or the subsequent reassembly of larger chain hydrocarbons. This result is consistent with the absence of Ag from the wide variety of metals that serve as Fischer–Tropsch catalysts.[50−52]

Once the Me group has migrated from a Au adatom to the Ag surface, the Me group could abstract a surface Ag atom and desorb into solution in an overall galvanic displacement reaction (MeAu(solution) + Ag(s) → MeAg(solution) + Au(s)). However, this reaction is endothermic by 55.9 kcal/mol. Not only is it more endothermic than Me decomposition, which is the most endothermic process of those described thus far, but the reaction energy even exceeds the Me decomposition activation barrier. Thus, the galvanic displacement reaction is unlikely to occur in this SPMCD system. The high endothermicity of the galvanic displacement reaction likely stems from the covalent nature of the Me–Au/Me–Ag bond which leads to the distinctly different behavior than that which arises from the ionic interactions between the $Au^{3+}/Ag^{+}$ ions and the $Cl^{-}$ ions of the $HAuCl_4$ precursors utilized in previously reported galvanic displacement reaction deposition techniques.[48,49]

*3.3.3. Role of Adsorbed Benzene Molecules.* Because of the elevated temperature of the SPMCSD process, a fraction of the Ag(111) surface will not be covered by adsorbed benzene molecules, although as mentioned above, vacant surface sites are unlikely to be adjacent to each other. Although ethane elimination can occur at bare 3-fold sites between adsorbed benzene molecules, benzene desorption increases the number of bare surface sites and thus increases the rate of ethane elimination. Ethane elimination between two adsorbed MeAu species at a site from which benzene has desorbed has a barrier of 27.4 kcal/mol relative to a monolayer of benzene and two separated adsorbed MeAu molecules. This is higher than the barrier for ethane elimination from neighboring MeAu species adsorbed in the interstitial space by the benzene adsorption energy of 14.3 kcal/mol. This barrier is low enough to be active at the 230 °C surface temperature and also lower than the solution-phase Au–P bond scission barrier and is thus not the rate-limiting step. Therefore, ethane elimination from neighboring adsorbed MeAu species either adsorbed within benzene vacancies or within interstices between adsorbed benzenes is a viable reaction pathway for SPMCSD.

We suggest that not only does adsorbed benzene limit the adsorption of $MeAuPPh_3$, but also it restricts the growth of Au particles. Adsorbed benzene hinders the migration of Au adatoms and adsorbed nanoparticles and also limits the size of contiguous bare Ag surface sites available for nanoparticle agglomeration. In order for Au nanoparticles to grow, either nanoparticles must travel across the surface and agglomerate or free Au atoms must attach to the nanoparticle. Free Au adatoms either result from the decomposition of adsorbed MeAu species or the escape of Au atoms from Au nanoparticles, which results in growth by Ostwald ripening when these adatoms add to larger Au nanoparticles. Diffusion of Au adatoms is restricted to hops between neighboring bare surface adsorption sites. Similarly, growth by particle agglomeration requires neighboring bare surface sites between which the particle can move, which requires that benzene molecules desorb to form pathways of bare surface along which Au particles migrate to a second Au particle and then merge. Au nanoparticle agglomeration involves nanoparticle migration along bare surface or over adsorbed benzene or desorption into solution. Each of these mechanisms requires benzene molecules to desorb to create a migration path for Au or for the Au clusters to break their strong Au–Ag bonds to the surface, making these processes highly unlikely. The only remaining viable pathway is atom-by-atom growth of nanoparticles, which is limited by the small number of available adatom diffusion paths between adsorbed benzene molecules. Furthermore, Au clusters larger than the size of bare surface between adsorbed benzenes are too large to form without benzene desorption, and thus steps in their growth at which the increase in their size requires desorption of an additional benzene molecule are penalized by the benzene desorption energy.

**3.4. Surface Decomposition of $MeAuPPh_3$ in the Absence of Solvent.** As described above, the adsorption of benzene to Ag(111) from the solvent significantly increases the energetic barriers of deposition mechanisms that proceed through molecular or dissociative adsorption of the large $MeAuPPh_3$ precursor. However, if a more weakly adsorbed solvent were used, more bare Ag sites would be available for precursor adsorption and the reaction energetics would be similar to that of reaction on bare Ag(111). For Au–P bond scission on bare Ag(111) we calculate an activation barrier and reaction energy of 9.4 and −5.0 kcal/mol, respectively, compared to the 38.5 kcal/mol barrier and reaction enthalpy of Au–P bond scission in solution. Thus, the Ag surface


DOI: 10.1021/acsami.5b01918
ACS Appl. Mater. Interfaces 2015, 7, 13384–13394

catalyzes Au−P dissociation and significantly accelerates the reaction. The schematic reaction potential energy surface is shown in Figure 6. As the Au−P bond of adsorbed $MeAuPPh_3$

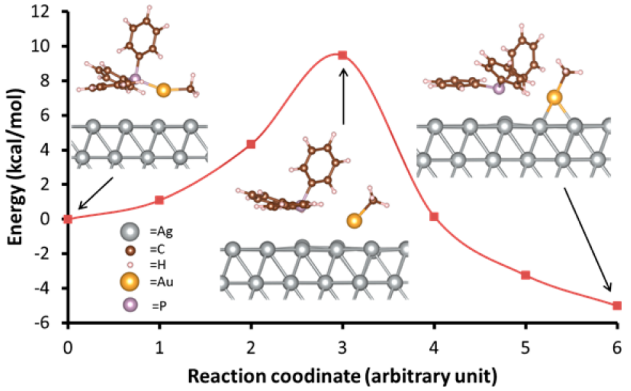


**Figure 6.** Potential energy surface for dissociation of the Au−P bond of the adsorbed $MeAuPPh_3$ precursor on the Ag(111) surface. The small white, medium brown, medium purple, large silver, and large yellow spheres represent H, C, P, Ag, and Au atoms, respectively.

dissociates, the phenyl groups of $PPh_3$ rotate to maximize their favorable dispersive interactions with the Ag surface. In fact, the formation of a P−Ag bond and the phenyl−Ag surface interactions are sufficiently favorable for the Au−P dissociation reaction to be slightly exothermic by $\Delta H_{rxn}$ = 5.0 kcal/mol. The low energy of the transition state stems from the attractive vdW interactions between the phenyl rings and the Ag surface as phenyl groups rotate away from their gas phase angles toward the surface. As the strong surface−phosphine favorable interactions suggest, the desorption of the $PPh_3$ phosphine into solution is endothermic by 46.2 kcal/mol. This indicates that, even at the high temperatures attained under SPMCSD conditions, $PPh_3$ is likely adsorbed on uncoated Ag surfaces. These results suggest that, for SPMCSD using this precursor, and a solvent that does not bind strongly to the Ag(111) surface, the precursor dissociation occurs on the surface at room temperature leading to Au deposition without SPR, and therefore loss of control of the Au nanoparticle deposition process.

## 4. DISCUSSION

During SPMCSD, $MeAuPPh_3$ dissociation likely occurs in solution because the 38.5 kcal/mol activation barrier for homogeneous dissociation is lower than the ≥42.9 kcal/mol activation barrier of the surface reaction. The high barrier for the reaction on the surface arises because three adsorbed benzene molecules must desorb prior to precursor adsorption, which is endothermic by 42.9 kcal/mol; the free energy barrier of 74.6 kcal/mol involves a significant entropic penalty to cluster three vacancies on the surface. Therefore, homogeneous Au−P bond dissociation with its 38.5 kcal/mol barrier is the lowest energy reaction path we identified. While this barrier is prohibitively high at 298 K, it is kinetically active at the near-surface temperatures generated by SPMCSD. Therefore, we suggest that $MeAuPPh_3$ decomposition proceeds through the following path: (1) $MeAu-PPh_3$ dissociation in the near-surface region with $E_{rxn}$ = 38.5 kcal/mol; (2) free MeAu adsorption to the Ag surface in hollow sites between adsorbed benzene molecules with $E_{rxn}$ = −39.6 kcal/mol; (3) ethane elimination and free Au atom formation with $E_{rxn}$ = −23.1 kcal/mol; and finally (4) nanoparticle formation from Au adatoms (Figure 7). Ethane formation from MeAu moieties occurs

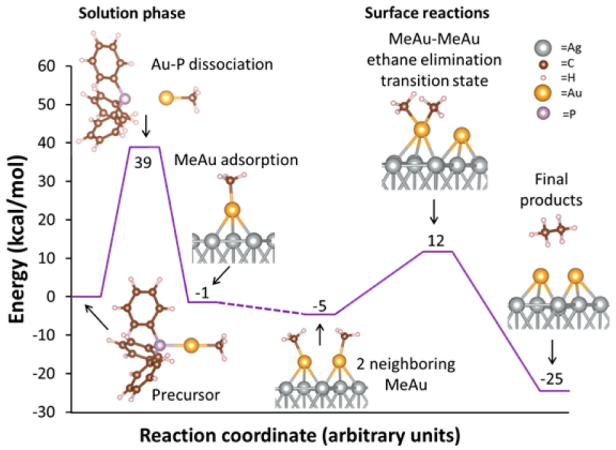


**Figure 7.** Schematic of the complete proposed reaction pathway for the SPMCSD of Au. The small white, medium brown, medium purple, large silver, and large yellow spheres represent H, C, P, Ag, and Au atoms, respectively.

either between adsorbed benzene molecules or at bare surface sites from which a benzene molecule has desorbed. Because the activation energy of the rate-limiting step for Au deposition in the presence of benzene is 38.5 kcal/mol, the solution-phase reaction can be initiated by heating. Additionally, SPR-mediated photothermal heating is limited to the near Ag surface region, and therefore reduces the formation of Au particles in the bulk solvent.

Adsorbed benzene molecules from the solvent act to block Ag surface sites and therefore inhibit the surface catalyzed $MeAuPPh_3$ decomposition pathway, which is low energy on bare Ag(111). This effect is similar to that observed for catalysts where competitive adsorption between species leads to surfaces partially covered by strongly adsorbed species that block active surface sites and thus poison the catalytic surface. For example, carbon monoxide binds strongly to various metal surfaces and can act as a poison in catalytic processes.[53−55] This effect can also be exploited to control the selectivity of various heterogeneous catalytic reactions; for example, Medlin and co-workers have used self-assembled alkanethiolate monolayers on catalysts to alter the selectivity of the furfural reduction reaction products by selectively eliminating reactant sites.[56] In the case of SPMCSD, instead of altering the final product distribution by intentionally adding competing adsorbates, the benzene solvent alters the reaction onset temperature by hindering the access of the precursor to the surface. Therefore, the homogeneous Au−P dissociation reaction, and therefore Au deposition, is triggered by increasing the near-surface temperature via SPR heating.

## 5. CONCLUSIONS

In this contribution we report an *ab initio* computational investigation of the mechanism of SPMCSD of Au nanoparticles on AgFON surfaces using $MeAuPPh_3$ as the precursor and benzene as the solvent. We found that benzene molecules adsorb strongly enough to the Ag surface to prevent the adsorption and subsequent dissociation of $MeAuPPh_3$ on the Ag surface. Our results show that $MeAuPPh_3$ homogeneously dissociates into MeAu and $PPh_3$ via a barrier of 38.5 kcal/mol


DOI: 10.1021/acsami.5b01918
ACS Appl. Mater. Interfaces 2015, 7, 13384−13394

and consequently occurs at the elevated temperatures generated by Ag SPR excitation in the near-surface region. If a $MeAuPPh_3$ molecule is in a region with a significantly SPR enhanced field and is reduced by a SPR excited electron, then its decomposition would be accelerated due to the lower Au−P scission energy of 27.2 kcal/mol for reduced $MeAuPPh_3$. MeAu fragments produced by precursor decomposition in solution then adsorb at exposed interstitial hollow sites of the Ag(111) surface between adsorbed benzene molecules and then decompose via binuclear reductive elimination to form ethane and Au adatoms, which subsequently cluster to produce nanoparticles on the Ag surface. Overall, the rate-limiting step for this mechanism is Au−P bond scission of $MeAuPPh_3$ in the solvent near the Ag surface where SPR-generated heat increases the temperature of the solution. In the absence of solvent, $MeAuPPh_3$ adsorbs to the Ag(111) surface and the Au−P scission activation energy decreases to 9.4 kcal/mol such that Au-based ethane elimination becomes the rate-limiting step with an activation energy of 11.7 kcal/mol, which is readily surmountable at room temperature, and therefore does not require additional heating by surface plasmons. Consequently, the effects of the benzene solvent on limiting precursor adsorption and subsequent reaction are critical to the control of SPMCSD of Au nanoparticles on Ag.

Understanding the effect of the phosphine substituents, and the solvent on each of the possible reaction pathways and thus their role in determining the active SPMCSD mechanism suggests the design of new SPMCSD precursors to enable greater control of the SPMCSD process and resulting nanostructures. For example, gold precursor complexes bearing phosphine ligands with smaller cone angles (e.g., $PMe_3$) should be small enough to adsorb to the bare surface sites in the interstitial space between adsorbed benzene molecules, or require only one surface benzene desorption. This precursor could then decompose on the Ag surface with a low overall activation energy, rather than in solution. The result would be elimination of ethane and deposition of Au nanoparticles at room temperature. In contrast, phosphine ligands that bind Au more strongly and possess sterically large substituents (e.g., $MeAuPPh_3$) will prevent adsorption between surface adsorbed solvent molecules, and thus require higher reaction temperatures or longer reaction times to deposit Au on Ag. This would enable better control of particle growth. The solvent can also be tuned so that larger solvent molecules that adsorb more weakly would desorb to provide more available sites for adsorption and surface reaction, enabling faster growth, growth at lower temperatures, or growth of larger particles. In contrast, smaller, more strongly adsorbing solvents would behave conversely. Through the detailed understanding of the Au SPMCSD mechanism developed here, new, additional highly controllable SPMCSD techniques could be developed by design of the precursor molecule and solvent, potentially leading to lower cost, bottom-up controllable nanoparticle deposition for electronic, chemical, and environmental applications.

## ■ ASSOCIATED CONTENT

### Supporting Information

Description of the method used for calculating the configurational entropy of the benzene vacancies, a cyclic voltammogram of $MeAuPPh_3$ and the associated experimental methods, and a table of the adsorption characteristics of $MeAuPPh_3$ as calculated using several functionals. The Supporting Information is available free of charge on the ACS Publications website at DOI: 10.1021/acsami.5b01918.

## ■ AUTHOR INFORMATION


### Corresponding Author

*E-mail: charles.musgrave@colorado.edu.

### Present Address

[‖]National Renewable Energy Laboratory, 15013 Denver West Parkway, Golden, CO 80401, United States.



### Funding

We thank the National Science Foundation for support under Grant CHE-1038015, the CCI Center for Nanostructured Electronic Materials. C.B.M. and A.M.H. thank the National Science Foundation for support through Grant CHE-1214131. W.D.W. and J.Q. greatly appreciate the support from the Air Force Office of Scientific Research under AFOSR Award No. FA9550-14-1-0304. C.L.M. greatly appreciates support from the National Science Foundation through Grant CBET-0966201 and the Department of Education through a Renewable and Sustainable Energy Graduate Assistance in Areas of National Need (GAANN) Fellowship.


### Notes

The authors declare no competing financial interest.

## ■ ACKNOWLEDGMENTS


This work utilized the Janus supercomputer, which is supported by the National Science Foundation through CNS-0821794 and the University of Colorado Boulder. Additionally, we would like to acknowledge that the images were created using the VESTA 3D visualization software.[57]


## ■ REFERENCES


(1) Sil, D.; Gilroy, K. D.; Niaux, A.; Boulesbaa, A.; Neretina, S.; Borguet, E. Seeing Is Believing: Hot Electron Based Gold Nanoplasmonic Optical Hydrogen Sensor. *ACS Nano* **2014**, *8*, 7755−7762.

(2) Qian, K.; Sweeny, B. C.; Johnston-Peck, A. C.; Niu, W.; Graham, J. O.; Duchene, J. S.; Qiu, J.; Wang, Y.-C.; Engelhard, M. H.; Su, D.; Stach, E. A.; Wei, W. D. Surface Plasmon-Driven Water Reduction: Gold Nanoparticle Size Matters. *J. Am. Chem. Soc.* **2014**, *136*, 9842−9845.

(3) Wang, F.; Li, C.; Chen, H.; Jiang, R.; Sun, L.-D.; Li, Q.; Wang, J.; Yu, J. C.; Yan, C.-H. Plasmonic Harvesting of Light Energy for Suzuki Coupling Reactions. *J. Am. Chem. Soc.* **2013**, *135*, 5588−5601.

(4) Bell, A. T. The Impact of Nanoscience on Heterogeneous Catalysis. *Science* **2003**, *299*, 1688−1691.

(5) Willets, K. A.; Van Duyne, R. P. Localized Surface Plasmon Resonance Spectroscopy and Sensing. *Annu. Rev. Phys. Chem.* **2007**, *58*, 267−297.

(6) Christopher, P.; Xin, H.; Linic, S. Visible-Light-Enhanced Catalytic Oxidation Reactions on Plasmonic Silver Nanostructures. *Nat. Chem.* **2011**, *3*, 467−472.

(7) Marimuthu, A.; Zhang, J. W.; Linic, S. Tuning Selectivity in Propylene Epoxidation by Plasmon Mediated Photo-Switching of Cu Oxidation State. *Science* **2013**, *339*, 1590−1593.

(8) Vazquez-Vazquez, C.; Vaz, B.; Giannini, V.; Perez-Lorenzo, M.; Alvarez-Puebla, R. A.; Correa-Duarte, M. A. Nanoreactors for Simultaneous Remote Thermal Activation and Optical Monitoring of Chemical Reactions. *J. Am. Chem. Soc.* **2013**, *135*, 13616−13619.

(9) Xie, W.; Walkenfort, B.; Schlucker, S. Label-Free SERS Monitoring of Chemical Reactions Catalyzed by Small Gold Nanoparticles Using 3D Plasmonic Superstructures. *J. Am. Chem. Soc.* **2013**, *135*, 1657−1660.

(10) Qiu, J.; Wu, Y.; Wang, Y.; Engelhard, M.; McElwee-White, L.; Wei, W. Surface Plasmon Mediated Chemical Solution Deposition of




DOI: 10.1021/acsami.5b01918
*ACS Appl. Mater. Interfaces* 2015, 7, 13384−13394

Gold Nanoparticles on a Nanostructured Silver Surface at Room Temperature. *J. Am. Chem. Soc.* **2013**, *135*, 38−41.
(11) Qiu, J.; Wei, W. D. Surface Plasmon-Mediated Photothermal Chemistry. *J. Phys. Chem. C* **2014**, *118*, 20735−20749.
(12) McElwee-White, L. Design of Precursors for the CVD of Inorganic Thin Films. *Dalton Trans.* **2006**, 5327−5333.
(13) McElwee-White, L.; Koller, J.; Kim, D.; Anderson, T. J. Mechanism-Based Design of Precursors for MOCVD. *ECS Trans.* **2009**, *25*, 161−171.
(14) Hemminger, O.; Marteel, A.; Mason, M. R.; Davies, J. A.; Tadd, A. R.; Abraham, M. A. Hydroformylation of 1-Hexene in Supercritical Carbon Dioxide Using a Heterogeneous Rhodium Catalyst. 3. Evaluation of Solvent Effects. *Green Chem.* **2002**, *4*, 507−512.
(15) Li, H.; Tang, Y.; Wang, Z.; Shi, Z.; Wu, S.; Song, D.; Zhang, J.; Fatih, K.; Zhang, J.; Wang, H.; Liu, Z.; Abouatallah, R.; Mazza, A. A Review of Water Flooding Issues in the Proton Exchange Membrane Fuel Cell. *J. Power Sources* **2008**, *178*, 103−117.
(16) Wong, A. L.; Harris, J. M. Surface Diffusion at the Liquid-Solid Interface: Quenching of Fluorescence from Pyrene Covalently Bound to Methylated Silica. *J. Phys. Chem.* **1991**, *95*, 5895−5901.
(17) Akpa, B. S.; D'Agostino, C.; Gladden, L. F.; Hindle, K.; Manyar, H.; McGregor, J.; Li, R.; Neurock, M.; Sinha, N.; Stitt, E. H.; Weber, D.; Zeitler, J. A.; Rooney, D. W. Solvent Effects in the Hydrogenation of 2-Butanone. *J. Catal.* **2012**, *289*, 30−41.
(18) Martin, G.; Mäki-Arvela, P.; Murzin, D.; Salmi, T. Solvent Effects in the Enantioselective Hydrogenation of Ethyl Benzoylformate. *Catal. Lett.* **2013**, *143*, 1051−1060.
(19) Nikoshvili, L.; Shimanskaya, E.; Bykov, A.; Yuranov, I.; Kiwi-Minsker, L.; Sulman, E. Selective Hydrogenation of 2-methyl-3-butyn-2-ol over Pd-nanoparticles Stabilized in Hypercrosslinked Polystyrene: Solvent Effect. *Catal. Today* **2015**, *241* (Part B), 179−188.
(20) Minder, B.; Mallat, T.; Pickel, K. H.; Steiner, K.; Baiker, A. Enantioselective Hydrogenation of Ethyl Pyruvate in Supercritical Fluids. *Catal. Lett.* **1995**, *34*, 1−9.
(21) Toukoniitty, E.; Mäki-Arvela, P.; Kuusisto, J.; Nieminen, V.; Päivärinta, J.; Hotokka, M.; Salmi, T.; Murzin, D. Y. Solvent Effects in Enantioselective Hydrogenation of 1-Phenyl-1,2-Propanedione. *J. Mol. Catal. A: Chem.* **2003**, *192*, 135−151.
(22) Augustine, R. L.; Warner, R. W.; Melnick, M. J. Heterogeneous Catalysis in Organic Chemistry. 3. Competitive Adsorption of Solvents During Alkene Hydrogenations. *J. Org. Chem.* **1984**, *49*, 4853−4856.
(23) Schmidt, M. W.; Baldridge, K. K.; Boatz, J. A.; Elbert, S. T.; Gordon, M. S.; Jensen, J. H.; Koseki, S.; Matsunaga, N.; Nguyen, K. A.; Su, S. J.; Windus, T. L.; Dupuis, M.; Montgomery, J. A. General Atomic and Molecular Electronic-Structure System. *J. Comput. Chem.* **1993**, *14*, 1347−1363.
(24) Zhao, Y.; Truhlar, D. The M06 suite of Density Functionals for Main Group Thermochemistry, Thermochemical Kinetics, Noncovalent Interactions, Excited States, and Transition Elements: Two New Functionals and Systematic Testing of Four M06-Class Functionals and 12 Other Functionals. *Theor. Chem. Acc.* **2008**, *120*, 215−241.
(25) Stevens, W. J.; Basch, H.; Krauss, M. Compact Effective Potentials and Efficient Shared-Exponent Basis Sets for the First- and Second-Row Atoms. *J. Chem. Phys.* **1984**, *81*, 6026−6033.
(26) Stevens, W. J.; Krauss, M.; Basch, H.; Jasien, P. G. Relativistic Compact Effective Potentials and Efficient, Shared-Exponent Basis Sets for the Third-, Fourth-, and Fifth-Row Atoms. *Can. J. Chem.* **1992**, *70*, 612−630.
(27) Ferrighi, L.; Hammer, B.; Madsen, G. K. H. 2D−3D Transition for Cationic and Anionic Gold Clusters: A Kinetic Energy Density Functional Study. *J. Am. Chem. Soc.* **2009**, *131*, 10605−10609.
(28) Li, H.; Pomelli, C. S.; Jensen, J. H. Continuum Solvation of Large Molecules Described by QM/MM: A Semi-iterative Implementation of the PCM/EFP Interface. *Theor. Chem. Acc.* **2003**, *109*, 71−84.
(29) Kresse, G.; Furthmüller, J. Efficient Iterative Schemes for Ab Initio Total-Energy Calculations Using a Plane-Wave Basis Set. *Phys. Rev. B* **1996**, *54*, 11169.
(30) Kresse, G.; Furthmüller, J. Efficiency of Ab-Initio Total Energy Calculations for Metals and Semiconductors Using a Plane-Wave Basis Set. *Comput. Mater. Sci.* **1996**, *6*, 15−50.
(31) Blöchl, P. E. Projector Augmented-Wave Method. *Phys. Rev. B* **1994**, *50*, 17953.
(32) Kresse, G.; Joubert, D. From Ultrasoft Pseudopotentials to the Projector Augmented-Wave Method. *Phys. Rev. B* **1999**, *59*, 1758−1775.
(33) Dion, M.; Rydberg, H.; Schröder, E.; Langreth, D. C.; Lundqvist, B. I. Van der Waals Density Functional for General Geometries. *Phys. Rev. Lett.* **2004**, *92*, 246401.
(34) Klimeš, J.; Bowler, D. R.; Michaelides, A. Chemical Accuracy for the Van der Waals Density Functional. *J. Phys.: Condens. Matter* **2010**, *22*, 022201.
(35) Marimuthu, A.; Zhang, J.; Linic, S. Tuning Selectivity in Propylene Epoxidation by Plasmon Mediated Photo-Switching of Cu Oxidation State. *Science* **2013**, *339*, 1590−1593.
(36) Mills, G.; Jónsson, H.; Schenter, G. K. Reversible Work Transition State Theory: Application to Dissociative Adsorption of Hydrogen. *Surf. Sci.* **1995**, *324*, 305−337.
(37) Häkkinen, H.; Landman, U. Gold Clusters ($Au_N$, $2<\sim N<\sim 10$) and Their Anions. *Phys. Rev. B* **2000**, *62*, R2287−R2290.
(38) Yu, B. D.; Scheffler, M. Physical Origin of Exchange Diffusion on fcc(100) Metal Surfaces. *Phys. Rev. B* **1997**, *56*, R15569−R15572.
(39) Kleiner, K.; Comas-Vives, A.; Naderian, M.; Mueller, J. E.; Fantauzzi, D.; Mesgar, M.; Keith, J. A.; Anton, J.; Jacob, T. Multiscale Modeling of Au-Island Ripening on Au (100). *Adv. Phys. Chem.* **2012**, 2011.
(40) Abad, E.; Dappe, Y. J.; Martínez, J. I.; Flores, F.; Ortega, J. $C_6H_6$/Au(111): Interface Dipoles, Band Alignment, Charging Energy, and Van der Waals Interaction, *J. Chem. Phys.* **2011**, *134*, -.
(41) Liu, W.; Carrasco, J.; Santra, B.; Michaelides, A.; Scheffler, M.; Tkatchenko, A. Benzene Adsorbed on Metals: Concerted Effect of Covalency and Van der Waals Bonding. *Phys. Rev. B* **2012**, *86*, 245405.
(42) Kelkkanen, A. K.; Lundqvist, B. I.; Nørskov, J. K. Van der Waals Effect in Weak Adsorption Affecting Trends in Adsorption, Reactivity, and the View of Substrate Nobility. *Phys. Rev. B* **2011**, *83*, 113401.
(43) Wellendorff, J.; Kelkkanen, A.; Mortensen, J.; Lundqvist, B.; Bligaard, T. RPBE-vdW Description of Benzene Adsorption on Au(111). *Top. Catal.* **2010**, *53*, 378−383.
(44) Rockey, T. J.; Yang, M.; Dai, H.-L. Adsorption Energies, Interadsorbate Interactions, and the Two Binding Sites within Monolayer Benzene on Ag(111). *J. Phys. Chem. B* **2006**, *110*, 19973−19978.
(45) Tamaki, A.; Kochi, J. K. Formation and Decomposition of Alkyl-Gold(I) Complexes. *J. Organomet. Chem.* **1973**, *61*, 441−450.
(46) Kale, M. J.; Avanesian, T.; Christopher, P. Direct Photocatalysis by Plasmonic Nanostructures. *ACS Catal.* **2014**, *4*, 116−128.
(47) Rakhimov, R. D.; Butin, K. P.; Grandberg, K. I. Redox Properties of Gold(I) Compounds with Organic Ligands. *J. Organomet. Chem.* **1994**, *464*, 253−260.
(48) Lu, X.; Tuan, H.-Y.; Chen, J.; Li, Z.-Y.; Korgel, B. A.; Xia, Y. Mechanistic Studies on the Galvanic Replacement Reaction between Multiply Twinned Particles of Ag and $HAuCl_4$ in an Organic Medium. *J. Am. Chem. Soc.* **2007**, *129*, 1733−1742.
(49) Sun, Y.; Xia, Y. Alloying and Dealloying Processes Involved in the Preparation of Metal Nanoshells through a Galvanic Replacement Reaction. *Nano Lett.* **2003**, *3*, 1569−1572.
(50) Khodakov, A. Y.; Chu, W.; Fongarland, P. Advances in the Development of Novel Cobalt Fischer−Tropsch Catalysts for Synthesis of Long-Chain Hydrocarbons and Clean Fuels. *Chem. Rev.* **2007**, *107*, 1692−1744.
(51) Dry, M. E. Present and Future Applications of the Fischer−Tropsch Process. *Appl. Catal., A* **2004**, *276*, 1−3.
(52) Maitlis, P. M. Fischer−Tropsch, Organometallics, and Other Friends. *J. Organomet. Chem.* **2004**, *689*, 4366−4374.
(53) Bartholomew, C. H. Mechanisms of Catalyst Deactivation. *Appl. Catal., A* **2001**, *212*, 17−60.
(54) McGown, W. T.; Kemball, C.; Whan, D. A.; Scurrell, M. S. Hydrogenation of Acetylene in Excess Ethylene on an Alumina


DOI: 10.1021/acsami.5b01918
*ACS Appl. Mater. Interfaces* 2015, 7, 13384−13394

Supported Palladium Catalyst in a Static System. *J. Chem. Soc., Faraday Trans.* **1977**, *73*, 632−647.
(55) Cheng, X.; Shi, Z.; Glass, N.; Zhang, L.; Zhang, J. J.; Song, D. T.; Liu, Z. S.; Wang, H. J.; Shen, J. A Review of PEM Hydrogen Fuel Cell Contamination: Impacts, Mechanisms, and Mitigation. *J. Power Sources* **2007**, *165*, 739−756.
(56) Pang, S. H.; Schoenbaum, C. A.; Schwartz, D. K.; Medlin, J. W. Directing Reaction Pathways by Catalyst Active-Site Selection Using Self-Assembled Monolayers, *Nat. Commun.* **2013**, *4*.
(57) Momma, K.; Izumi, F. VESTA 3 for Three-Dimensional Visualization of Crystal, Volumetric and Morphology Data. *J. Appl. Crystallogr.* **2011**, *44*, 1272−1276.


DOI: 10.1021/acsami.5b01918
*ACS Appl. Mater. Interfaces* 2015, 7, 13384−13394